Published in final edited form as:
J Endocrinol. 2011 April ; 209(1): 21–32. doi:10.1530/JOE-10-0308.

Targeted ablation of the PTH/PTHrP receptor in osteocytes impairs bone structure and homeostatic calcemic responses

William F. Powell Jr.[1], **Kevin J. Barry**[1], **Irena Tulum**[1], **Tatsuya Kobayashi**[1], **Stephen E. Harris**[2], **F. Richard Bringhurst**[1], and **Paola Divieti Pajevic**[1,#]

[1]Endocrine Unit, Massachusetts General Hospital and Harvard Medical School, Boston MA

[2]Department of Periodontics, University of Texas Health Science Center School of Dentistry, San Antonio, TX

Abstract

Parathyroid hormone (PTH) is a major physiologic regulator of calcium, phosphorous and skeletal homeostasis. Cells of the osteoblastic lineage are key targets of PTH action in bone, and recent evidence suggests that osteocytes might be important in the anabolic effects of PTH. To understand the role of PTH signaling through the PTH/PTHrP receptors (PPR) in osteocytes and to determine the role(s) of these cells in mediating the effects of the hormone, we have generated mice in which PPR expression is specifically ablated in osteocytes. Transgenic mice in which the 10Kb-*Dmp1* promoter drives a tamoxifen-inducible Cre –recombinase were mated with animals in which exon1 of PPR is flanked by Lox-P sites. In these animals, osteocyte-selective PPR knockout (Ocy-PPR^{cKO} mice) could be induced by administration of tamoxifen. Histological analysis revealed a reduction in trabecular bone and mild osteopenia in Ocy-PPR^{cKO} mice. Reduction of trabeculae number and thickness was also detected by μCT analysis whereas BV/TV% was unchanged. These findings were associated with an increase in Sost and sclerostin expression. When Ocy-PPR^{cKO} mice were subjected to a low calcium diet, to induce secondary hyperparathyroidism, their blood calcium levels were significantly lower than littermate controls. Moreover, PTH was unable to suppress Sost and sclerostin expression in the Ocy-PPR^{cKO} animals, suggesting an important role of PTH signaling in osteocytes for proper bone remodeling and calcium homeostasis.

Keywords

osteocytes; parathyroid hormone; parathyroid hormone receptor

Introduction

Osteocytes are the most abundant cells in bone, outnumbering osteoblasts by 10-fold and osteoclasts by 1000-fold (Aguirre, et al. 2006) and yet their function is still incompletely understood. Osteocytes act as mechanosensors of bone, and recent evidence has indicated a role for these cells in bone modeling and remodeling and phosphate homeostasis (Feng, et

Corresponding Author: Paola Divieti Pajevic Endocrine Unit, Thier 1101, Massachusetts General Hospital, 50 Blossom Street, Boston MA 02114, USA. Phone :(617)726-6184; Fax:(617)726-7543; divieti@helix.mgh.harvard.edu.

Disclosure Statement: The Authors have nothing to disclose

Declaration of Interest: The Authors have nothing to disclose

Authors Contribution: PDP, WFP and FRB planned and designed the experiments, WFP, KJB and PDP performed experiments, IT performed the immunohistochemical analysis. TK provided the PPRfl/fl mice, SHE provided the 10Kb-*Dmp1*-Cre-ERT2 plasmid, PDP and WFP analyzed the data. PDP, WFP and FRB wrote the manuscript.

al. 2006; Lorenz-Depiereux, et al. 2006; Tatsumi, et al. 2007). Studies on osteocytes have been hampered by the inaccessibility of these cells and by the lack of molecular and cell surface markers that could be used to isolate and characterize them. In the last decade, however, our knowledge of osteocytes has expanded dramatically, mostly as a result of the identification of several selective osteocytic markers, such as dentin matrix protein 1 (DMP-1) (George, et al. 1994; Yang, et al. 2005; Ye, et al. 2004), matrix extracellular phosphoglycoprotein / osteocyte-factor 45 (MEPE/OF45) (Gowen, et al. 2003; Petersen, et al. 2000), membrane-type matrix metalloproteinase (MT1-MMP) (Holmbeck, et al. 1999; Holmbeck, et al. 2005), Phex (Liu, et al. 2006; Westbroek, et al. 2002) and sclerostin (Sost) (van Bezooijen, et al. 2004; Winkler, et al. 2003) that have allowed, for the first time, a more direct analysis of the molecular and cellular biology of osteocytes.

Osteocytes express receptors for several extracellular ligands, including the parathyroid hormone (PTH) type 1 receptor (PPR) (Fermor and Skerry 1995), estrogen receptors (both α and β) (Ehrlich, et al. 2002; Jessop, et al. 2004; Lanyon, et al. 2004; Lee, et al. 2004), prostaglandin receptor (EP_2) and a novel, yet uncloned, receptor that specifically recognizes the carboxyl-terminal region of PTH, the carboxyl-terminal PTH receptor (CPTHR) (Divieti, et al. 2005; Divieti, et al. 2001).

PTH, a single-chain polypeptide comprised of 84 amino acids, is synthesized and secreted by the parathyroid glands in a calcium-regulated manner. PTH maintains serum calcium homeostasis and controls renal phosphate reabsorption and vitamin D 1a-hydroxylation. PTH modulates bone turnover by actions that are mediated by a G-protein coupled receptor, the PPR (Juppner, et al. 1991). The PPR is highly expressed in bone and kidney, but is also found in a variety of other tissues not regarded as classical PTH targets. This likely reflects the local paracrine role of PTHrP in tissues such as breast, skin, heart, blood vessels and others. The N-terminal 34 amino-acids of PTH are necessary and sufficient to fully activate the PPR, which, in turn, can activate multiple G protein-coupled pathways, including those that signal through cAMP/Protein kinase A (PKA), phospholipase C (PLC)/Protein kinase C (PKC), and nonPLC-dependent PKC and Ca^{++}_i.

It has been shown that PTH can prevent apoptosis of osteocytes (and osteoblasts) and that this mechanism may contribute to the anabolic action of intermittently administered PTH (Jilka, et al. 1998; Jilka, et al. 1999). Moreover, recent studies from O'Brien et al. (O'Brien, et al. 2006) revealed a critical role of PTH (and PPR) in osteocytes. They generated transgenic mice expressing a constitutively active PPR specifically in osteocytes by placing the H223R mutant receptor (Schipani, et al. 1995; Schipani, et al. 1997) under the control of the 8Kb-*Dmp1* promoter (named DMP1-caPTHR1). In these mice the levels of *Sost* mRNA in bone were 3-fold lower than wild type littermates at 8 weeks of age. Strikingly, DMP1-caPTHR1 mice also exhibited a 42% and an 84% increase in BMD in the spine and femur, respectively, as determined by DEXA (O' Brien et al. 2006), suggesting an important role for PPR/cAMP mediated pathways in the anabolic effect of PTH.

With this in mind, we aimed to specifically ablate the PPR in osteocytes to directly assess the role of receptor activation in these cells. We have generated transgenic mice in which the 10-Kb promoter of *Dmp1* drives a tamoxifen-inducible bacteriophage Cre-recombinase. These mice were crossed with mice in which exon 1 of the PPR gene was flanked by lox-P sites to generate animals that specifically lack PPRs in osteocytes. Initial histological analysis demonstrated that lack of PPR expression in osteocytes induce a reduction in trabecular bone, accompanied by a tonic elevation of *Sost* and sclerostin and a lack of PTH-induced *Sost* and sclerostin suppression.

Moreover, ablation of PPR in osteocytes impairs skeletal responses to a low calcium diet, indicating a critical role of this receptor in controlling calcium homeostasis.

Materials & Methods

Mice

Generation of the 10Kb-*Dmp1*-Cre-ERT2 mice—The 14-kB *Dmp1* promoter fragment (-9624 ~ +4439) – containing a 9624-bp promoter region, a 95-bp exon1(E1), 4326-bp intron 1 and 17-bp initial non-coding region of exon 2 (E2) - was cloned into the Cre-ERT2-LacZ-MH vector, which contains the Cre-ERT2 DNA. The *Dmp1*-Cre-ERT2 transgene was released from the vector backbone with the use of the unique restriction enzymes NotI and SalI, purified by Qiaquick gel extraction kit (Qiagen, Valencia, CA, USA), quantified and microinjected into the pronucleus of B6C3F1 Hybrid mice (Taconic, Hudson, NY, USA) to generate founder mice. Injections were performed on site at the Massachusetts General Hospital transgenic core facility (CBRC MGH mouse facility). Three rounds of pronuclear injections were performed and a total of 68 offspring were obtained. Eighteen pups died at birth and 14 of the remaining 50 were positive for Cre-recombinase integration (23%), as assessed by genomic PCR of tail DNA using Cre-specific primers (Figure 1B). Six independent transgenic founders were mated with wild-type C57BL/6 mice, and the F1 offspring were analyzed. All transgenic lines produced pups at the expected 1:1 ratio and the pups appeared normal, grew indistinguishably from wild-type and were fertile. To further analyze the characteristics of these mice, a Southern Blot analysis of genomic DNA was performed. A Cre-recombinase specific probe was cloned using PCR primers, as shown in Figure 1A. Genomic DNA was digested using the restriction enzyme EcoRI that cleaves the insert in one site and Southern Blot analysis confirmed the germline transmission and single site of insertion. In addition, to assess that the transgene was transmitted through generations, Southern Blot analysis of genomic DNA from F2 progenies was performed, as shown in Supplemental Figure 1. PPR-floxed mice were described previously (Kobayashi, et al. 2005). 10Kb-*Dmp1*-Cre-ERT2 mice were crossed with homozygous PPR-floxed ($PPR^{fl/fl}$) mice to obtain doubly heterozygous mice 10Kb-*Dmp1*-Cre-ERT2:$PPR^{fl/+}$ which were in turn mated with $PPR^{fl/fl}$ to obtained the desired 10Kb-*Dmp1*-Cre-ERT2:$PPR^{fl/fl}$, or "Ocy-PPR^{cKO}," mice and littermates which include 10Kb-*Dmp1*-Cre-ERT2:$PPR^{fl/+}$, $PPR^{fl/fl}$, and $PPR^{fl/+}$, all of which were used as controls in all experiments.

We crossed the *Dmp1*-Cre-ERT2 mice with ROSA26R mice (Soriano 1999), kindly provided by Dr. Henry Kronenberg (Massachusetts General Hospital, Boston, MA), to obtain the ROSA26R and *Dmp1*-Cre-ERT2 double transgenic mice for monitoring Cre-recombinase expression.

For tamoxifen injections, 10 mg of free base tamoxifen (MPBio, Solon OH, USA) was dissolved in 100μl of dimethylformamide (Fisher Scientific, Waltham, MA, USA) and then diluted to 10 mg/ml in corn oil (Sigma, St. Louis, MO, USA). Mice were injected with 50 to 150μl, depending on their ages.

Genotyping of mice

The genotypes of the mice were determined by PCR analysis of genomic DNA extracted from tail biopsies. For the 10Kb-*Dmp1*-Cre-ERT2 transgene, the forward Cre primer (5′CGCGGTCTGGCAGTAAAAACTATC-3′) and the reverse Cre primer (5′-CCCACCGTCAGTACGTGAGATATC-3′) were used to generate a PCR product of approximately 400bp. For the floxed PPR allele, the P1 primer (5′-ATG AGG TCT GAG GTA CAT GGC TCT GA -3′) and the P2 primer (5′-CCT GCT GAC CTC TCT GAA AGA ATG T -3′) were used, which recognized the sequence spanning the 3′lox-P site, as

previously reported (Kobayashi, et al. 2002). Wild-type and mutant alleles give ~ 210 bp and 290 bp products, respectively. Mice were primarily kept in mixed genetic backgrounds with dominance of the C57/Bl6 and all experiments were performed with littermates as controls. Procedures that involved mice were approved by the Institutional Animal Care and Use Committee, Subcommittee on Research Animal Care, at Massachusetts General Hospital. Allele specific DNA recombination was performed on DNA isolated from long bones (femurs), calvaria, kidney, liver, skeletal muscle and spleen. Briefly, pups were treated with tamoxifen (400-500 μg) and day 3, 5, 7, 14 and 21. Mice were euthanized at three weeks of age by CO2 inhalation, tissues were quickly removed and DNA was isolated following standard protocol. Multiplex PCR analysis was performed using allele specific primers, P1, P2 and P3 (5′ACA TGG CCA TGC CTG GGT CTG AGA 3′) and following the manufacturer protocol (Quiagen™ Multiplex PCR kit, Quiagen Valencia, CA USA)

Histology and immunohistochemistry

Tissues were fixed in 10% formalin/PBS solution at 4°C ON, decalcified in 20% EDTA pH 8 for 7-15 days, processed, embedded in paraffin, and sectioned. Sections were stained with hematoxylin and eosin, or used for immunohistochemistry. In some experiments, undecalcified femurs were embedded in methylmethacrylate (Aldrich Chemical Co, Milwuakee, WI, USA). Sections were cut using a diamond-embedded wire saw, and then stained by the Von Kossa method. Sclerostin expression was detected immunohistochemically using commercially available biotinylated anti-mouse sclerostin antibody (1: 50 dilution) (R&D Systems Inc., Minneapolis, MN, USA) and DAB detection (Vector, Burlingame, CA, USA). Briefly, sections were deparaffinized, and endogenous peroxidase activity was inhibited by 3% H2O2 treatment for 15 min. Subsequently, slides were blocked with TNB (TSA ™ Biotin Tyramide Kit, Perkin Elmer, Waltham MA, USA) for 30 min at RT and then incubated for 1 h with biotinylated anti-mouse sclerostin antibody. After extensive rinsing, sections were incubated for 30 min with streptavidin(SA) conjugated horseradish peroxidase (HRP) and tyramide following the manufactures protocol (TSA ™ Biotin Tyramide Kit) and developed with a 3,3′-diaminobenzidine substrate-chromogen system (Vector laboratories, Burlingame, CA, USA).

Serology

Blood was collected by tail vein bleeding for ionized calcium and by carotid transection or retro-orbital bleeding for serum collection. Ionized calcium was measured by the Ciba-Corning 634 Ca++/pH analyzer (Ciba-Corning Diagnostics Corp., Medfield, MA, USA). Intact immunoreactive PTH was measured in duplicate using ELISA (Immutopics Inc., San Clemente, CA, USA). Serum mouse TRAP5B (Mouse TRAP Assay), PINP and CTX (Rat-LAPS EIA) were measured in duplicate using ELISA (Immunodiagnostic Systems Limited, Boldon, UK). Statistical analysis was performed using the Student's *t* test, and *P* values less than 0.05 were accepted as significant.

Low calcium diet and PTH injections

In some experiments, mice were fed a low calcium diet (0.02% calcium, 0.4% phosphorous, Teklad, Harlan, Madison WI, USA) for two weeks prior to calcium measurement. Mice were injected subcutaneously with 300μg/kg of human PTH(1-34) (MGH Peptide Core Facility). Blood was collected by tail bleeding for ionized calcium measurement before and 1 hr after PTH injections using a Ca++/pH analyzer.

RNA extraction and purification

RNA was isolated from long bones of Ocy-PPR^{cKO} mice and littermate controls following sequential collagenase and EDTA digestions to remove endosteal and periosteal osteoblasts

and bone marrow cells. For detailed protocol see Supplemental Data. Femurs were washed with 1 ml of RNA-later solution (Ambion, Austin, TX, USA) prior to RNA isolation by Trizol. RNA was extracted from the bone by homogenizing it in Trizol (Invitrogen, Carlsbad, CA, USA) using a tissue homogenizer for 1 minute on ice. The RNA was then extracted from the homogenate according to the manufacturer's recommendations. RNA quality and quantity was ascertained by UV spectrophotometry (NanoDrop 8000, Thermo Fisher, Waltham MA USA).

Quantitative RT-PCR

Reverse transcription was performed on 0.5-1 μg of DNAse-treated total RNA and oligoDT primers using Omniscript (Invitrogen Carlsbad, CA, USA) according to the manufacturer's instructions. Quantitative PCR was performed using the QuantiTect SYBR Green PCR Kit (QIAGEN, Valencia CA, USA) and the DNA Engine Opticon 2 qPCR system (MJ Research Inc., Waltham, MA, USA). The comparative method, using the –ΔΔCT formula, was used to determine the RNA relative expression, glyceraldehyde-3-phosphate dehydrogenase (GAPDH) being used for normalizing. Statistical analysis was performed using the Student's *t* test, and *P* values less than 0. 05 were accepted as significant. Primer sequences are described in Supplemental Data.

Cyclic AMP measurement

Tibiae were isolated from four to six week old mice mouse. Briefly, tibiae were dissected and cleaned of adherent tissues. Distal and proximal epiphyses were removed and the bone marrow was flushed out using 2-3 ml of αMEM supplemented with 0.1 % bovine serum albumin, BSA and 25mM Hepes pH 7.4). The remaining diaphysial enriched region of the bones was cut into three pieces and sequentially digested as described above for RNA isolation. Each piece was then placed in ice-cold cAMP-assay buffer (Dulbecco Modified Essential Medium containing 10 mM HEPES, 0.1% heat-inactivated BSA and 1 mM isobutylmethylxantine). Bone pieces were then incubated in cAMP-assay buffer with the appropriate treatment at 37°C for 15 min. The three pieces of each tibia were incubated with vehicle alone (assay buffer), 100nM human PTH (1-34) or 0.1μM M forskolin. At the end of the incubation, the reaction was terminated by quickly removing the bones and placing them in 0.3 ml of cold 90% 2-propanol in 0.5 M HCl. Bones were then incubated for 16-18 h at 4°C. Propanol extraction was repeated, and the combined extracts were evaporated by vacuum centrifugation. The dried extracts were redissolved in acetate buffer (50 mM Na acetate/0.05% Na azide, pH 6.2) for measurement of cAMP by a specific RIA, as previously described (38). Bones were washed twice with 0.5 ml acetone and once with 0.5 ml ether and were air-dried and weighed. The results were normalized for the bone weight, and the data were expressed as picomole of cAMP produced per mg of dry bone. Each experiment was repeated at least three times.

FACS Analysis

In some experiments homozygous *Dmp1*-GFP transgenic mice (provided by Drs. Ivo Kalajzic and David W. Rowe, University of Connecticut Health Center, Hartford, CN) were crossed with PPRfl/fl mice to generate Ocy-PPR^{ckO} and WT mice that express GFP under the 8K*b-Dmp1* promoter. Calvarial cells obtained from mice exhibiting the same genotype were pooled and GFP-expressing cells (enriched in osteocytes) were separated from GFP-negative cells (enriched in osteoblasts) by immediately subjecting the cell suspension to sorting using a fluorescence-activated cell sorting (FACS) using an Aria flow cytometer (BD Biosciences, San Jose, CA, USA) at the Massachusetts General Hospital Flow Cytometry Core Facility.

Bone Mineral Density (BMD) DXA

Mouse BMD was measured by dual-energy x-ray absorptiometry using a Lunar PIXImus II densitometer (GE Medical System Luna, Madison, WI). In brief, mice were sacrificed, right femurs and vertebral bodies were fixed overnight in 10% buffered formalin and then preserved in 70% ethanol. The excised right femurs and vertebral bodies (region L4-L5) were used to determine bone mineral content (BMC, g) and bone mineral density (BMD, g/cm^2).

MicroCT analysis

Assessment of bone morphology and microarchitecture was performed using a desktop high-resolution μCT (μCT40, Scanco Medical, Brüttisellen, Switzerland), as described previously (Bouxsein, et al.). In brief, the distal femoral metaphysis and L_5 vertebral body were scanned using an X-ray energy of 70 KeV, integration time of 200 ms, and a 12-μm isotropic voxel size. For the cancellous bone region, we assessed bone volume fraction (BV/TV, %), trabecular thickness (Tb.Th, μm), trabecular separation (Tb.Sp, μm), trabecular number (Tb.N, 1/mm), connectivity density (Conn.D, 1/mm^3), and structure model index (SMI).

Statistical Analysis

All data are presented as mean ± standard deviation (S.D.). The statistical significance of differences between groups was determined by Student's t-test. P value les than 0.05 were accepted as significant.

Results

Generation and Characterization of 10Kb-Dmp1-Cre-ERT2 transgenic mice

10Kb-*Dmp1*-Cre-ERT2 animals were generated as described Material and Methods To test the efficiency and specificity of the lines **generated**, the 10Kb-*Dmp1*-Cre-ERT2 animals were intercrossed with the homozygous ROSA26R reporter mice (Soriano 1999). ROSA26R mice have a floxed stop-cassette upstream of the LacZ gene. In the presence of Cre-recombinase activity, the stop-cassette is excised, LacZ is expressed and β-galactosidase (β-gal) activity can be detected using the 5-bromo-4-chloro-3-indoyl -D-galactopyranoside (X-Gal) staining procedure. Three-day old 10Kb-*Dmp1*-Cre -ERT2/ROSA26R mice were exposed to intraperitoneal injections of tamoxifen (50-60μg/gr) at days 3, 5 and 7, and then maintained on a weekly injection of 5-10μg/gr of tamoxifen for an additional 2 weeks. After X-Gal staining, calvarial bones and hindlimbs were embedded in paraffin and stained with eosin. In some experiments, kidneys were also evaluated for X-gal staining. As shown in Figure 2A-C for calvaria (DP1-cre positive: A top panel and B at 40X and DMP1-cre negative: A bottom panel and C at 40X) and Figure 2D-F for long bone (femur of DMP1-cre positive: D top panel and E at 40X and DMP1-cre negative: D bottom panel and F at 40X) for one founder, most of the osteocytes were positive for the X-Gal staining (Figures 2A and D, top panels and Figures B and E), while no staining was present in *Dmp1*-Cre negative controls (Figures 2A and D, bottom panels and Figures C and F), in kidneys, bone marrow or skeletal muscle of DMP1-Cre positive (Supplemental Figure 1A, C and D) or in *Dmp1*-Cre positive animals not treated with tamoxifen (data not shown). Under this regimen, we calculated that 77± 9 % of osteocytes stained blue for X-gal activity (81.3 ± 3 % in calvaria; 72.6 ± 6 % in tibias and 78.5 ± 1.1 % in femurs), indicating excision of the flox-stop codon in the *lacZ* promoter region in these cells. In addition, to further assess the specificity of the promoter, we calculated the percentage of X-gal positive endosteal and periosteal osteoblasts. Under the regimen described above, 8.6 ± 6.8 % of calvaria osteoblasts and 1.1± 1 % of femoral osteoblasts were positive for X-gal staining, indicating that only a minority

of mature osteoblasts express the 10Kb *Dmp1*-promoter. Initial analysis showed that two of the six lines demonstrated highly penetrant excision of the ROSA26R stop cassette and we focused our experiments in these two lines.

In another set of experiments, 3-4 week old mice were injected with 5-10μg/gr of tamoxifen 3 times a week for 2-4 weeks before analyzing PPR expression by real-time quantitative-PCR (qPCR). The efficiency of PPR ablation, as assessed by qPCR in mRNA derived from collagenase digested long bones, with this tamoxifen regimen was again around 60-70%, and was comparable to the one described above (Figure 3 A), indicating that the receptor can be successfully ablated in adult mice.

DMP1-CreERt2 model effectively and specifically decreases -PPR expression in osteocytes

10Kb-*Dmp1*-Cre-ERT2 mice were crossed with homozygous PPR-floxed mice, as described in Methods, to obtain double heterozygotes that were in turn mated with $PPR^{fl/fl}$ to obtain 10Kb-*Dmp1*-Cre-ERT2:$PPR^{fl/fl}$ or "Ocy-PPR^{cKO} " mice and littermate controls.

10Kb-*Dmp1*-Cre-ERT2:$PPR^{fl/+}$ females were time-mated with $PPR^{fl/fl}$ males and injected intraperitoneally with 2mg of tamoxifen at 17.5 days post-coitus. Pups were sacrificed 1 day after birth, genoptyped, and long bones were excised and analyzed histologically. As anticipated, given the short interval between tamoxifen induction and sacrifice, we did not observe any macroscopic phenotype in the Ocy-PPR^{cKO} pups, nor any overt osteocyte phenotype in the calvarial and long bones of these mice compared with littermate controls. Immunohistochemical analysis using anti-sclerostin antibody showed no differences in expression between Ocy-PPR^{cKO} and littermate calvaria and long bones after three days of exposure to tamoxifen.

To ascertain the successful deletion of PPR from osteocytes in response to the tamoxifen regimen, we first carried out qPCR analysis for PPR expression. Mice, both Ocy-PPR^{cKO} and littermate controls, were injected with tamoxifen at day 3, 5 and 7 and then weekly, as described above. We performed real-time qPCR for the PPR using primers specific for the floxed E1 region. As shown in Figure 3A, Ocy-PPR^{cKO} femurs had a 64% reduction in PPR expression compared to littermate controls (results are expressed as percentage of control and are normalized by GAPDH). To further evaluate PPR ablation in a pure osteocytic population, we generated Ocy-PPR^{cKO} and control mice that express GFP under the 8Kb-DMP1 promoter by mating the $PPR^{fl/fl}$ mice with the 8Kb-DMP1-GFP mice. Newborn pups were genotyped and then injected with 50μg/gr of tamoxifen at days 2 and 4 postnatally. Primary calvarial cells were then isolated by 8 sequential collagenase and EDTA digestions, and cells derived from fractions 3-8 were sorted, as described in Materials and Methods. As shown in Figure 3B, PPR expression was reduced by 80% in GFP-positive cells from Ocy-PPR^{cKO} animals compared to littermate controls (control 100±8.8 %, Ocy-PPR^{cKO}: 23.1±0.27%, control-GFP neg = 48.1±17.5% and Ocy-PPR^{cKO} -GFP neg 52.7±8.8%, results are expressed as percentage of control and are normalized for GAPDH expression). There was no significant difference in PPR expression in GFP-negative cells compared to Ocy-PPR^{cKO} and control animals (osteoblasts). These results demonstrate that the PTH receptor ablation is specific for osteocytes and that it can be induced upon tamoxifen administration. Interestingly, receptor expression in control GFP-positive cells (osteocytes) is two-fold that of GFP-negative cells (osteoblasts), suggesting higher receptor expression in osteocytes than osteoblasts.

In addition, allele-specific DNA recombination for the PPR locus was evaluated by PCR using primer spanning the floxed E1 region. As shown in Figure 1C, the DNA recombination (lower band) was observed only in the skeletal tissues such as long bones

(bone-marrow depleted femurs) and calvaria, whereas no recombination was detected in kidney, spleen muscle and liver, indicating that the PPR ablation was specific for osteocytes.

Functional Consequences of Deletion of the PPR gene in Osteocytes

To assess functional ablation of the PPR in osteocytes, we measured PTH-induced cyclic AMP accumulation in osteoblast/marrow-cell-depleted bone explants, enriched in osteocytes, from Ocy-PPR^{cKO} and littermate controls. Tibiae were isolated from four to five week old Ocy-PPR^{cKO} and control littermates injected with tamoxifen (50-60μg/gr) at days 3,5 and 7 postnatally and then weekly with 5-10μg/gr, as described for the ROSA26R experiments. As shown in Figure 3C, there was a statistically significant reduction (86.8 % reduction) of cyclic AMP accumulation in response to PTH in Ocy-PPR^{cKO} osteocyte enriched bone fragments, compared to littermate controls (Ocy-PPR^{cKO} = 6.16± 9.6 picomol/mg bone vs control = 46.9±16.2 picomol/mg bone; $p<0.05$). As a positive control, no difference was detected in the response to forskolin (Ocy-PPR^{cKO} = 43.4±13.8 picomol/mg bone vs littermate controls = 36.7±23.9 picomol/mg bone) indicating an intact adenylyl-cyclase machinery in these osteocyte-enriched bone fragments. To assess that PPR ablation was confined to osteocytes and not osteoblasts, we performed cAMP accumulation in response to PTH in primary calvarial cells (predominantly composed of osteoblasts) isolated from 4-5 day old Ocy-PPR^{cKO} and littermate controls. As shown in Figure 3D, cAMP accumulation in calvarial osteoblasts from Ocy-PPR^{cKO} was indistinguishible from littermate controls, indicating that PPR-ablation was specific for osteocytes.

Moreover primary calvaria cells isolated from 4-5 day old Ocy-PPR^{cKO} and littermate controls were treated with 100nM hPTH(1-34) for 4 hr and RANKL expression was assessed by qPCR. As expected, RANKL was significantly upregulated in both Ocy-PPR^{cKO} and littermate controls (7.6± 2.5 and 18. 5± 1.8 fold respectively) indicating that osteoblasts in Ocy-PPR^{cK0} do have intact PTH responsiveness.

To further assess the phenotype of mice lacking PPR in osteocytes, we proceeded to analyze adult mice. Four to six week old mice were injected with tamoxifen (20-30μg/gr) three times a week for four weeks. At the end of the 4 weeks, mice were acutely challenged with a single subcutaneous injection of human PTH(1-34) (300μg/kg) and sacrificed after 1 hour. As shown in Figure 4A, sclerostin expression (assessed immunohistochemically) was markedly reduced in the tibiae of littermate control animals following PTH administration, but was readily detectable in tibiae of Ocy-PPR^{cKO} animals (Figure 4B), demonstrating no PTH-induced sclerostin inhibition in Ocy-PPR^{cKO} mice. We also analyzed Sost mRNA expression by real-time PCR and Ocy-PPR^{cKO} mice showed no acute reduction of Sost expression after PTH injection, whereas controls showed more than a 40% acute down-regulation of Sost mRNA expression (Figure 4C). Moreover, Ocy-PPR^{cKO} also displayed a significantly overall increase in Sost expression of more than 54%, as detected by real-time qPCR (control = 90±20 vs Ocy-PPR^{cKO} 147±33% n=9; $p<0.01$) (Figure 4D) as well as a suppression of Wnt-signaling pathways as demonstrated by a significant reduction of Axin-2 mRNA (control = 109±47 vs Ocy-PPR^{cKO} 65±25% n=7; $p<0.05$) (Figure 4E).

We then analyzed the bone phenotype of Ocy-PPR^{cKO} and littermate controls. Hematoxylin and eosin staining of decalcified tibias demonstrated a reduction of trabecular bone and a delay in the secondary ossification center. Furthermore, Von Kossa staining of plastic (Figure 5 A and B) sections confirmed a reduction of the trabecular bone. We measured bone mineral density (BMD) in isolated femurs and vertebral bodies (L4-L5) by DEXA (Piximus) in both females and males. In Ocy-PPR^{cKO} females there was a significant reduction of both vertebral and femoral BMD (Figure 5 C and D). Males also tended to have a lower BMD compared to littermate controls, but this was not significantly different.

To investigate if the low BMD in Ocy-PPR^{cKO} mice was due to a reduction in osteoblast activity, an increase in osteoclast activity or a combination of both, we measured markers of bone resorption and bone formation in control and Ocy-PPR^{cKO} mice, as shown in Table 1. Serum levels of collagen type 1 fragment were indistinguishable between Ocy-PPR^{cKO} and control littermates (PINP: controls n=17 70,3 ± 51.2 ng/mL ; Ocy-PPR^{cKO} n=14 74.9 ± 55.2 ng/mL), whereas CTX were slightly elevated in KO mice compared to controls (controls n=9 9.07 ± 5.03 ng.mL ; Ocy-PPR^{cKO} n=11 13.8 ± 6.7 ng/mL) although they were not statistically different. Finally TRAP5b was not significantly different between control and Ocy-PPR^{cKO} mice (TRAP5b controls n=16 1.51 ± 0.78 U/L; Ocy-PPR^{cKO} n=12 1.08 ± 0.44 U/L), suggesting that rates of bone modeling and remodeling are relatively normal in these mice. To further evaluate the bone architecture of Ocy-PPR^{cKO} mice, we performed μCT analysis of trabecular bone both in males and females. As shown in Table 2, Ocy-PPR^{cKO} tended to have lower trabecular bone compared to controls (reduced connectivity density, SMI and trabeculae number) although this was not statistically significant indicating that ablation of PPR in osteocytes induce mild skeletal abnormalities, as assessed by μCT.

Finally, to further analyze PPR KO in osteocytes we subjected six-week old mice to two weeks of low calcium diet (0.02% calcium) to induce secondary hyperparathyroidism. Mice were pre-treated with tamoxifen (20-30μg/gr three times a week) 1 week before starting the diet and during the 2 weeks of the diet. Ionized calcium was measured at the beginning of the study (before starting tamoxifen injections) and was not significantly different among groups. At the end of the 3 weeks, mice were sacrificed and blood and skeletal specimens were collected and analyzed as described above. Plasma PTH levels in these mice were elevated (190.7± 82 pg/ml and 294.8±124 pg/ml for control and Ocy-PPR^{cKO,} respectively), confirming that secondary hyperparathyroidism had been achieved. Interestingly, Ocy-PPR^{cKO} animals displayed significantly lower ionized and total calcium levels compared to littermate controls (which included DMP1-Cre:PPR $^{fl/fl}$ not treated with tamoxifen and tamoxifen-treated DMP1-Cre:PPR$^{fl/+}$ and PPR $^{fl/fl}$) (Figure 6A, B and Table 1). Similar results were also obtained in a separate set of experiments using younger mice, treated with tamoxifen from day 3 postnatally, to ablate PPRs at an earlier time data not shown. In these mice tamoxifen was administered at days 3, 5, 7, 14 and 21 postnatally and mice were fed a low calcium diet at day 21 for an additional 2 weeks. In addition, PPR expression in the kidneys of these animals was evaluated to ascertain that the receptor was fully expressed in this organ. We did not observe any difference in PPR mRNA levels between Ocy-PPR^{cKO} and littermate controls, indicating that the lower serum calcium level was not likely due to altered renal responsiveness to circulating PTH.

Discussion

Osteocytes are believed to play a key role in skeletal mechanosensing whereby they modulate bone modeling and remodeling in response to changes in shear or strain forces. Moreover, recent studies (O'Brien et al. 2006) demonstrated that mice in which the constitutively active PPR is expressed in osteocytes display a dramatic increase in trabecular bone, indicating an important role of PTH and the PPR in osteocytes.

To investigate the role of PTH and related molecules in osteocytes *in vivo*, we have generated mice in which the receptor is selectively and temporary ablated in these cells. We used the 9.6 Kb of the DMP1- promoter to drive a tamoxifen-inducible Cre-recombinase in mice in which exon-1 of the PPR is flanked by Lox-P sites. Ocy-PPR^{cKO} mice were born with the expected Mendelian ratio, were viable and were indistinguishable from littermate controls, indicating that the Cre-recombinase was not expressed in the absence of tamoxifen induction. The 10Kb-DMP1-cre-ERT2 recombinase was exclusively and specifically expressed in osteocytes and in rare bone lining cells (less tan 8% of total endosteal

osteoblasts), as demonstrated by ROSA26 experiments. The promoter was readily inducible and the efficiency of Cre-recombinase excision was around 70-80%. The transgene was heritable as assessed by Southern blot analysis of F2 generation of the original founders.

Initial characterization of the Ocy-PPR^{cKO} mice revealed a slight growth retardation (data not shown) that was associated with a mild osteopenic phenotype, as assessed by histological analysis of long bones and by DEXA measurement. Interestingly, vertebral and femoral BMD (as assessed by Piximus) was significantly lower than littermate controls only in females, suggesting a potential effect of gender on PTH action on osteocytes. Moreover, when bone microarchitecture was analyzed by μCT, there was no significant difference between the Ocy-PPR^{cKO} and littermate controls (although the KO mice displayed lower Conn. Dens, SMI and Tb.N) suggesting that the bone abnormalities in Ocy-PPR^{cKO} are mild. One possible explanation for the discrepancy between DEXA and μC T is the different area of bone that is routinely analyzed by these two techniques.

In Ocy-PPR^{cKO} mice, Sost and sclerostin expression was significantly higher than in littermate controls, indicating that the osteopenia might be a consequence of suppression of the wnt-bcatenin signaling pathway in osteocytes, as demonstrated by a significant suppression of Axin-2 mRNA expression (Figure 4D) in Ocy-PPR^{cKO}. Sclerostin, the secreted protein product of the SOST gene, is expressed exclusively by osteocytes and has emerged as a potent indirect negative regulator of bone osteoblastogenesis (van Bezooijen et al. 2004; van Bezooijen, et al. 2005; Winkler et al. 2003). Transgenic mice overexpressing Sost show low bone mass (Winkler et al. 2003) whereas Sost-null animals have high bone mass. Sclerostin acts by binding the low-density lipoprotein receptor 5 and 6 (LRP5 and 6) and inhibits wnt-βcatenin signaling pathway (Ai, et al. 2005). Also, the high bone mass mutation of Lrp5, G171V, binds less efficiently to sclerostin. Inhibition of wnt-βcatenin in osteocytes, in turn, somehow suppresses osteoblast proliferation and function. Several studies have proven that the wnt-βcatenin pathway is critical for proper bone metabolism, as again revealed by loss-of-function or gain-of-function mutations of LRP5 that cause, respectively, Osteoporosis-Pseudoglioma Syndrome (OPS) or high bone mass (HBM) syndrome, in humans and rodents (Gong, et al. 2001). Our data suggest that PTH exerts its anabolic effect on bone, at least in part, by suppressing sclerostin expression in osteocytes and therefore releasing the wnt-βcatenin inhibition. In our mouse model, lack of PTH signaling in osteocytes is associated with an increase in sclerostin expression, inhibition of wnt-βcatenin and ultimately osteopenia. These findings are in agreement with recent studies of O'Brien et al. (O'Brien, et al. 2008), who demonstrated that mice expressing a constitutively active PPR receptor (Calvi, et al. 2001 ; Schipani et al. 1995) specifically in osteocytes have a dramatic decrease in Sost expression and a 40% increase in BMD. Moreover, these transgenic mice could potentially rescue the osteopenic phenotype of LRP5-/- animals, if Lrp5 and/or 6 play direct roles in osteocyte biology. This would clearly indicate that osteocyte-derived sclerostin is indeed a negative regulator of wnt-βcatenin signaling. Recently, Yadav et al. (Yadav, et al. 2008) reported that Lrp5 acts on bone via regulation of serotonin synthesis in the gut and that the main action of LRP5 is in the duodenum. The authors demonstrated that LRP5 acts on serotonin-producing cells in the gut by blocking an enzyme that converts the amino acid tryptophan to serotonin. This new connection between bone and gut-derived serotonin, although shifting the action of LRP5 from osteoblasts to the duodenum, does not exclude that osteocyte-secreted sclerostin functions as a negative regulator of the wnt-βcatenin pathways in osteoblasts. Additional studies will be needed to investigate the role of serotonin in osteocytes.

Interestingly, the Ocy-PPR^{cKO} mice also demonstrated hypocalcemia when challenged with a low calcium diet, suggesting an important role of osteocytes in regulating calcium ion homeostasis. Normally, this low calcium diet is easily corrected by increased PTH

production and increased remodeling to bring the calcium back to normal. However, when osteocytes lack a functional PPR, this does not happen. This suggests that the osteocyte **might be** important in regulating calcium through PTH signaling. The role of osteocytes in controlling calcium homeostasis is controversial. Osteocytes clearly express high levels of receptors for PTH, and the osteocyte lacuno-canalicular network constitutes a microcirculatory system for calcium-containing periosteocytic fluid that is distinct from blood plasma and lymph fluid (Knothe Tate 2003). The osteocyte network represents an enormous surface area over which the cells interface with the surrounding matrix, useful for matrix mineral access (Cullinane 2002). Osteocytes can serve as key regulators of calcium homeostasis, are distributed widely in bone matrix, and are ideally situated to engage in systemic calcium homeostasis. Here we report that mice lacking the PPR specifically in osteocytes have an impaired calcium homeostasis when subjected to a low calcium diet and fail to properly respond to secondary hyperparathyroidism. These data support this hypothesis. However, it should be considered that three organs participate in supplying calcium to the blood: (I) the small intestine, through the absorption of calcium from the diet (vitamin-D dependent); (II) the kidney, through the reabsorption of calcium from the glomerular filtrate; and (III) the skeleton, with the release of calcium from the bone. PTH acts directly, or indirectly, on these target organs, but the mechanism by which the hormone rapidly (within 1-2 hrs) increases blood calcium concentration is not completely understood. Several hypotheses have been postulated which include an increase in renal calcium reabsorption from the kidney, an increase in bone resorption and/or an increase in intestinal calcium absorption. Finally, our data support the theory that a release of calcium from the osteocytic lacuno-canalicular network may also be very important in this process, and regulated by PTH.

In summary, we have generated mice in which the PPR can be specifically ablated from osteocytes upon tamoxifen administration. These mice displayed mild osteopenia, tonic increase in Sost and sclerostin expression and lack of PTH-induced *Sost* and sclerostin suppression. Moreover, Ocy-PPR^{cKO} mice were unable to maintain a normal calcium plasma level when subjected to a low calcium diet.

Supplementary Material

Refer to Web version on PubMed Central for supplementary material.

Acknowledgments

Funding: This work was supported by the National Institutes of Health grants DK079161 (PDP), P01AR46798 (SEH) and by an MGH-ECOR Interim grant (PDP).

References

Aguirre JI, Plotkin LI, Stewart SA, Weinstein RS, Parfitt AM, Manolagas SC, Bellido T. Osteocyte apoptosis is induced by weightlessness in mice and precedes osteoclast recruitment and bone loss. J Bone Miner Res. 2006; 21:605–615. [PubMed: 16598381]

Ai M, Holmen SL, Van Hul W, Williams BO, Warman ML. Reduced affinity to and inhibition by DKK1 form a common mechanism by which high bone mass-associated missense mutations in LRP5 affect canonical Wnt signaling. Mol Cell Biol. 2005; 25:4946–4955. [PubMed: 15923613]

Bouxsein ML, Boyd SK, Christiansen BA, Guldberg RE, Jepsen KJ, Muller R. Guidelines for assessment of bone microstructure in rodents using micro-computed tomography. J Bone Miner Res. 25:1468–1486. [PubMed: 20533309]

Calvi LM, Sims NA, Hunzelman JL, Knight MC, Giovannetti A, Saxton JM, Kronenberg HM, Baron R, Schipani E. Activated parathyroid hormone/parathyroid hormone-related protein receptor in

osteoblastic cells differentially affects cortical and trabecular bone. J Clin Invest. 2001; 107:277–286. [PubMed: 11160151]

Cullinane DM. The role of osteocytes in bone regulation: mineral homeostasis versus mechanoreception. J Musculoskelet Neuronal Interact. 2002; 2:242–244. [PubMed: 15758444]

Divieti P, Geller AI, Suliman G, Juppner H, Bringhurst FR. Receptors specific for the carboxyl-terminal region of parathyroid hormone on bone-derived cells: determinants of ligand binding and bioactivity. Endocrinology. 2005; 146:1863–1870. [PubMed: 15625242]

Divieti P, Inomata N, Chapin K, Singh R, Juppner H, Bringhurst FR. Receptors for the carboxyl-terminal region of pth(1-84) are highly expressed in osteocytic cells. Endocrinology. 2001; 142:916–925. [PubMed: 11159865]

Ehrlich PJ, Noble BS, Jessop HL, Stevens HY, Mosley JR, Lanyon LE. The effect of in vivo mechanical loading on estrogen receptor alpha expression in rat ulnar osteocytes. J Bone Miner Res. 2002; 17:1646–1655. [PubMed: 12211435]

Feng JQ, Ward LM, Liu S, Lu Y, Xie Y, Yuan B, Yu X, Rauch F, Davis SI, Zhang S, et al. Loss of DMP1 causes rickets and osteomalacia and identifies a role for osteocytes in mineral metabolism. Nat Genet. 2006; 38:1310–1315. [PubMed: 17033621]

Fermor B, Skerry TM. PTH/PTHrP receptor expression on osteoblasts and osteocytes but not resorbing bone surfaces in growing rats. J Bone Miner Res. 1995; 10:1935–1943. [PubMed: 8619374]

George A, Gui J, Jenkins NA, Gilbert DJ, Copeland NG, Veis A. In situ localization and chromosomal mapping of the AG1 (Dmp1) gene. J Histochem Cytochem. 1994; 42:1527–1531. [PubMed: 7983353]

Gong Y, Slee RB, Fukai N, Rawadi G, Roman-Roman S, Reginato AM, Wang H, Cundy T, Glorieux FH, Lev D, et al. LDL receptor-related protein 5 (LRP5) affects bone accrual and eye development. Cell. 2001; 107:513–523. [PubMed: 11719191]

Gowen LC, Petersen DN, Mansolf AL, Qi H, Stock JL, Tkalcevic GT, Simmons HA, Crawford DT, Chidsey-Frink KL, Ke HZ, et al. Targeted disruption of the osteoblast/osteocyte factor 45 gene (OF45) results in increased bone formation and bone mass. J Biol Chem. 2003; 278:1998–2007. [PubMed: 12421822]

Holmbeck K, Bianco P, Caterina J, Yamada S, Kromer M, Kuznetsov SA, Mankani M, Robey PG, Poole AR, Pidoux I, et al. MT1-MMP-deficient mice develop dwarfism, osteopenia, arthritis, and connective tissue disease due to inadequate collagen turnover. Cell. 1999; 99:81–92. [PubMed: 10520996]

Holmbeck K, Bianco P, Pidoux I, Inoue S, Billinghurst RC, Wu W, Chrysovergis K, Yamada S, Birkedal-Hansen H, Poole AR. The metalloproteinase MT1-MMP is required for normal development and maintenance of osteocyte processes in bone. J Cell Sci. 2005; 118:147–156. [PubMed: 15601659]

Jessop HL, Suswillo RF, Rawlinson SC, Zaman G, Lee K, Das-Gupta V, Pitsillides AA, Lanyon LE. Osteoblast-like cells from estrogen receptor alpha knockout mice have deficient responses to mechanical strain. J Bone Miner Res. 2004; 19:938–946. [PubMed: 15190886]

Jilka RL, Weinstein RS, Bellido T, Parfitt AM, Manolagas SC. Osteoblast programmed cell death (apoptosis): modulation by growth factors and cytokines. J Bone Miner Res. 1998; 13:793–802. [PubMed: 9610743]

Jilka RL, Weinstein RS, Bellido T, Roberson P, Parfitt AM, Manolagas SC. Increased bone formation by prevention of osteoblast apoptosis with parathyroid hormone. J Clin Invest. 1999; 104:439–446. [PubMed: 10449436]

Juppner H, Abou-Samra AB, Freeman M, Kong XF, Schipani E, Richards J, Kolakowski LF Jr, Hock J, Potts JT Jr, Kronenberg HM, et al. A G protein-linked receptor for parathyroid hormone and parathyroid hormone-related peptide. Science. 1991; 254:1024–1026. [PubMed: 1658941]

Knothe Tate ML. “Whither flows the fluid in bone?” An osteocyte's perspective. J Biomech. 2003; 36:1409–1424. [PubMed: 14499290]

Kobayashi T, Chung UI, Schipani E, Starbuck M, Karsenty G, Katagiri T, Goad DL, Lanske B, Kronenberg HM. PTHrP and Indian hedgehog control differentiation of growth plate chondrocytes at multiple steps. Development. 2002; 129:2977–2986. [PubMed: 12050144]

Kobayashi T, Soegiarto DW, Yang Y, Lanske B, Schipani E, McMahon AP, Kronenberg HM. Indian hedgehog stimulates periarticular chondrocyte differentiation to regulate growth plate length independently of PTHrP. J Clin Invest. 2005; 115:1734–1742. [PubMed: 15951842]

Lanyon L, Armstrong V, Ong D, Zaman G, Price J. Is estrogen receptor alpha key to controlling bones' resistance to fracture? J Endocrinol. 2004; 182:183–191. [PubMed: 15283679]

Lee KC, Jessop H, Suswillo R, Zaman G, Lanyon LE. The adaptive response of bone to mechanical loading in female transgenic mice is deficient in the absence of oestrogen receptor-alpha and -beta. J Endocrinol. 2004; 182:193–201. [PubMed: 15283680]

Liu S, Zhou J, Tang W, Jiang X, Rowe DW, Quarles LD. Pathogenic role of Fgf23 in Hyp mice. Am J Physiol Endocrinol Metab. 2006; 291:E38–49. [PubMed: 16449303]

Lorenz-Depiereux B, Bastepe M, Benet-Pages A, Amyere M, Wagenstaller J, Muller-Barth U, Badenhoop K, Kaiser SM, Rittmaster RS, Shlossberg AH, et al. DMP1 mutations in autosomal recessive hypophosphatemia implicate a bone matrix protein in the regulation of phosphate homeostasis. Nat Genet. 2006; 38:1248–1250. [PubMed: 17033625]

O'Brien, C.; PL, I.; K, V.; PE, C.; G, AR.; G, JJ.; J, C.; R, S.; W, RS.; E, S., et al. American Society for Bone and Mineral Research. Ed JoBa M Research; Philadelphia. PA: 2006. Activation of PTH Receptor 1 Specifically in Osteocytes Suppresses Sost Expression and Increases Bone Mass in Transgenic Mice.

O'Brien CA, Plotkin LI, Galli C, Goellner JJ, Gortazar AR, Allen MR, Robling AG, Bouxsein M, Schipani E, Turner CH, et al. Control of bone mass and remodeling by PTH receptor signaling in osteocytes. PLoS ONE. 2008; 3:e2942. [PubMed: 18698360]

Petersen DN, Tkalcevic GT, Mansolf AL, Rivera-Gonzalez R, Brown TA. Identification of osteoblast/osteocyte factor 45 (OF45), a bone-specific cDNA encoding an RGD-containing protein that is highly expressed in osteoblasts and osteocytes. J Biol Chem. 2000; 275:36172–36180. [PubMed: 10967096]

Schipani E, Kruse K, Juppner H. A constitutively active mutant PTH-PTHrP receptor in Jansen-type metaphyseal chondrodysplasia. Science. 1995; 268:98–100. [PubMed: 7701349]

Schipani E, Lanske B, Hunzelman J, Luz A, Kovacs CS, Lee K, Pirro A, Kronenberg HM, Juppner H. Targeted expression of constitutively active receptors for parathyroid hormone and parathyroid hormone-related peptide delays endochondral bone formation and rescues mice that lack parathyroid hormone-related peptide. Proc Natl Acad Sci U S A. 1997; 94:13689–13694. [PubMed: 9391087]

Soriano P. Generalized lacZ expression with the ROSA26 Cre reporter strain. Nat Genet. 1999; 21:70–71. [PubMed: 9916792]

Tatsumi S, Ishii K, Amizuka N, Li M, Kobayashi T, Kohno K, Ito M, Takeshita S, Ikeda K. Targeted ablation of osteocytes induces osteoporosis with defective mechanotransduction. Cell Metab. 2007; 5:464–475. [PubMed: 17550781]

van Bezooijen RL, Roelen BA, Visser A, van der Wee-Pals L, de Wilt E, Karperien M, Hamersma H, Papapoulos SE, ten Dijke P, Lowik CW. Sclerostin is an osteocyte-expressed negative regulator of bone formation, but not a classical BMP antagonist. J Exp Med. 2004; 199:805–814. [PubMed: 15024046]

van Bezooijen RL, ten Dijke P, Papapoulos SE, Lowik CW. SOST/sclerostin, an osteocyte-derived negative regulator of bone formation. Cytokine Growth Factor Rev. 2005; 16:319–327. [PubMed: 15869900]

Westbroek I, De Rooij KE, Nijweide PJ. Osteocyte-specific monoclonal antibody MAb OB7.3 is directed against Phex protein. J Bone Miner Res. 2002; 17:845–853. [PubMed: 12009015]

Winkler DG, Sutherland MK, Geoghegan JC, Yu C, Hayes T, Skonier JE, Shpektor D, Jonas M, Kovacevich BR, Staehling-Hampton K, et al. Osteocyte control of bone formation via sclerostin, a novel BMP antagonist. Embo J. 2003; 22:6267–6276. [PubMed: 14633986]

Yadav VK, Ryu JH, Suda N, Tanka K, Gingrich JA, Shutz G, Glorieux FH, Chaing CY, Zajac JD, Insogna KI, et al. Lrp5 Controls Bone Formation by Inhibiting Serotonin Synthesis in the Duodenum. Cell. 2008; 135:825–837. [PubMed: 19041748]

Yang W, Lu Y, Kalajzic I, Guo D, Harris MA, Gluhak-Heinrich J, Kotha S, Bonewald LF, Feng JQ, Rowe DW, et al. Dentin matrix protein 1 gene cis-regulation: Use In osteocytes to characterize local responses to mechanical loading in vitro and In vivo. J Biol Chem. 2005

Ye L, MacDougall M, Zhang S, Xie Y, Zhang J, Li Z, Lu Y, Mishina Y, Feng JQ. Deletion of dentin matrix protein-1 leads to a partial failure of maturation of predentin into dentin, hypomineralization, and expanded cavities of pulp and root canal during postnatal tooth development. J Biol Chem. 2004; 279:19141–19148. [PubMed: 14966118]

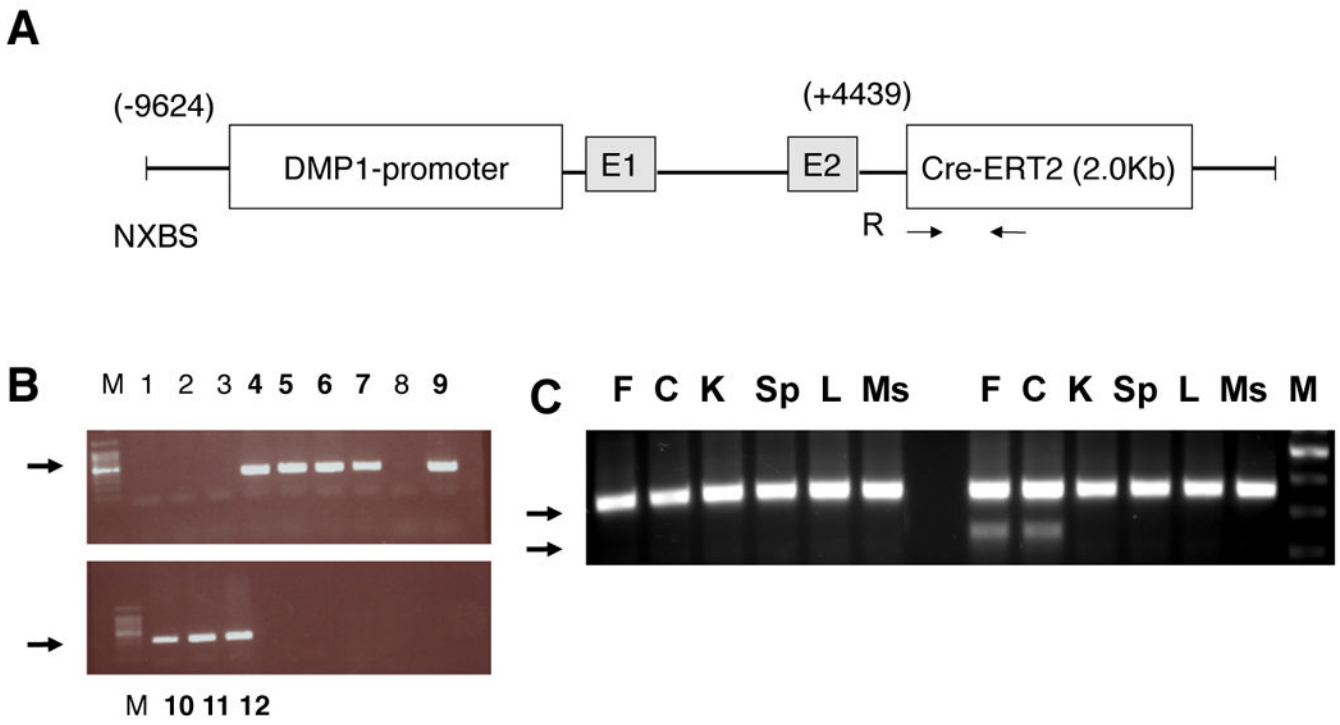

Figure 1. Generation of 10KbDMP1-Cre-ERT2 mice

A) The 9.6Kb of DMP1 was cloned into the SK plasmid. NXBS and R are unique restriction sites N=NotI, X=Xbe. B=BmH, S=SmaI. R= EcoRI. The vector was released by NotI-SalI digestion. E1 and E2 are Exon 1 and the portion of Exon2 before the ATG initiation site, respectively. Arrows indicate approximate sites of PCR primers for Cre-recombinase. B) Genomic DNA from founders was assessed for integration of Cre recombinase by PCR using primers specific for the Cre-ERT2 region (arrows). Genomic DNA from the second round of pronuclear injections is shown. Eight mice were positive for Cre-recombinase (lanes 4-7, 9-12). M=100bp ladder. H = no DNA control (water). Arrows indicate the expected Cre product (size 300bp). C) Allele specific DNA recombination PCR in control (left lines) and Ocy-PPR^{cKO} (right lines) mice. A specific band (~ 600) is present only in femur (F) and calvaria (C) of Ocy-PPR^{cKO}. The presence of the larger band (~1.5 Kb) is due to contamination with other bone cells (i.e. bone marrow cells, osteoblasts and osteoclasts) that were not removed during DNA preparation. As shown here, there was no recombination in kidney (K), spleen (Sp), liver (L) or muscle (Ms). M = 100bp marker.

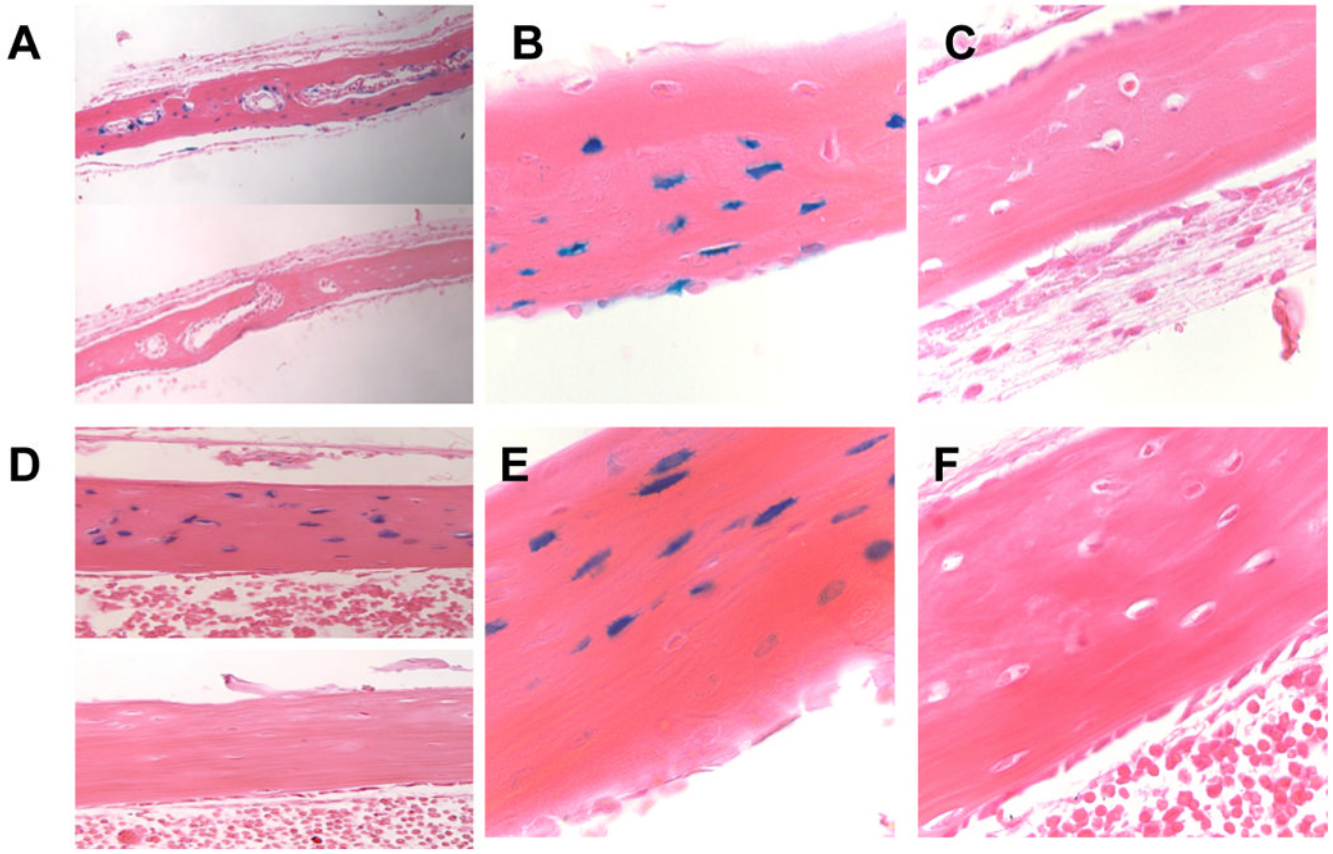

Figure 2. Characterization of DMP1-Cre-ET2 mice

X-gal staining of 5 weeks old calvarial (A-C) and long bones (femur)(D-F) from Rosa26:10KbDMP1-Cre-positive (A top panel and B: calvaria ; D top panel and E: femur) and Cre-negative (A bottom panel and C: calvaria; D bottom panel and F; femur) mice. Animals were injected with tamoxifen at days 3,5, 7, 14 and 21 days postnatal and sacrificed at 23 days (2 days after last tamoxifen injection). Panel A and D: 20X magnification; panel B,C,E and F : 40X magnification.

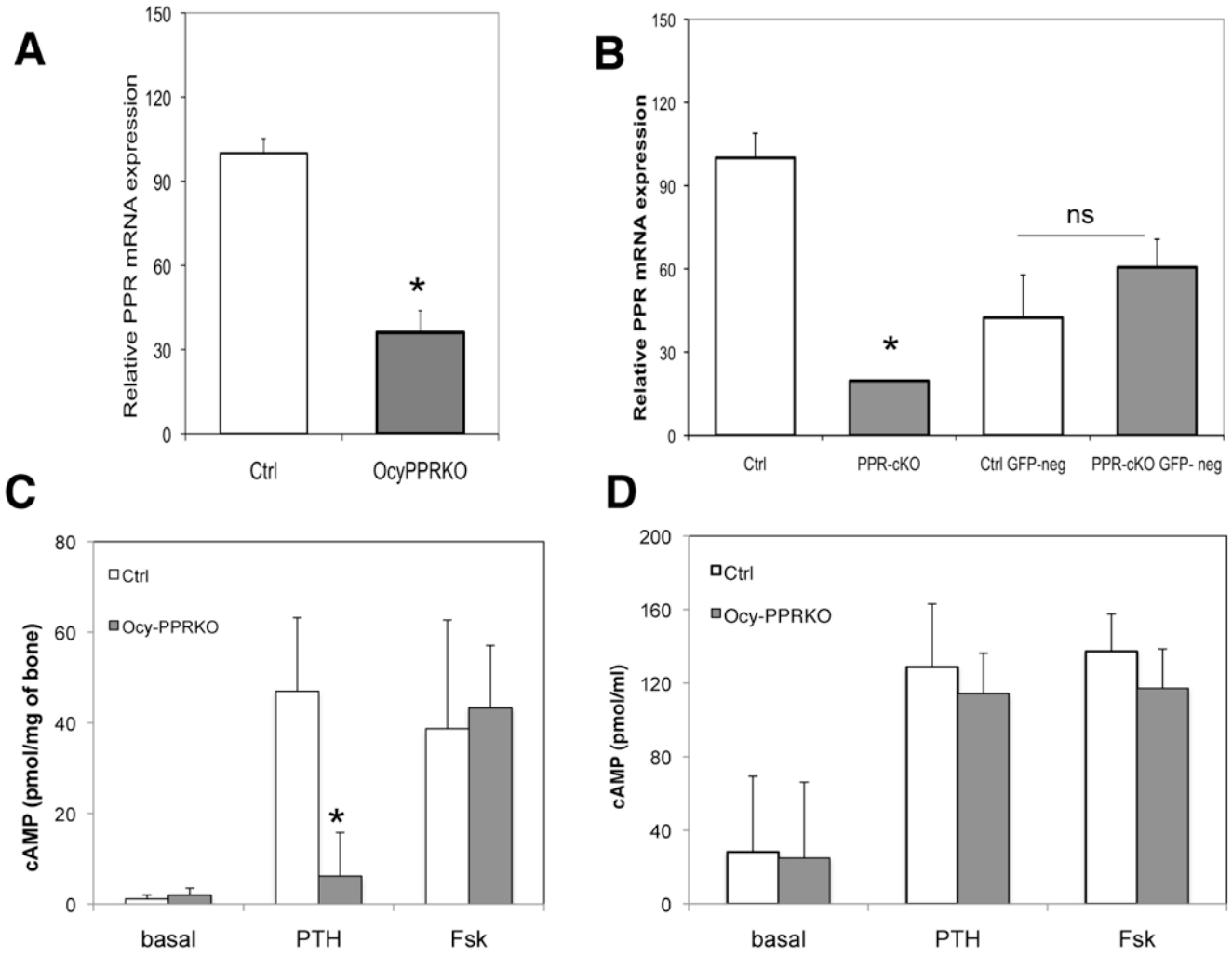

Figure 3. PPR ablation in osteocytes

Realtime qPCR from A) RNA extracted from femurs of 5 week old littermate controls (Ctrl, n=3) and Ocy-PPR^{cKO} (n=3) mice. Data are expressed as relative mRNA, using the –ΔΔCT formula, normalized by GAPDH and expressed as percentage of controls. PPR expression in the Ocy-PPR^{cKO} is decreased to 36.1 ± 7.7 % of controls. Data are expressed as mean ± SD of triplicates. * $p<0.05$. Representative experiment. B) Realtime qPCR of RNA extracted from sorted GFP-positive and GFP negative calvarial cells derived from Ocy-PPR^{cKO} (PPR-cKO) and control littermates (Ctrl). Data are expressed as percentage of controls and are corrected for GAPDH. PPR expression in GFP-positive Ocy-PPR^{cKO} osteocytes (PPR-KO) is decreased by 80% compared to littermate control GFP-positive osteocytes (Ctrl) (two left-most bars). PPR expression in GFP-negative cells (osteoblasts) from controls and Ocy-PPR^{cKO} animals is not significantly different (two right-most bars). Data are expressed as mean ± SD of triplicates. * $p<0.05$. Representative experiment. C) Cyclic AMP accumulation in bone-marrow deprived, collaged-digested tibial explants. Right tibias of 5 week old Ocy-PPR^{cKO} (n= 3, black bars) and control littermates (n=4, grey bars) were assayed for their *in vitro* responsiveness to 100nM hPTH(1-34) or 10μM forskolin (Fsk). Data are expressed as pmol of cAMP/mg of bone. Data are expressed as mean ± SD of triplicates * $p<0.002$ Ocy-PPR^{cKO} vs WT. D) Cyclic AMP accumulation in primary calvaria cells. Primary calvarial cells from 4-5 days old pups were were assayed for their *in vitro*

responsiveness to 100nM hPTH(1-34) or 10μM forskolin (Fsk). Data are expressed as pmol cAMP/well. Data are expressed as mean ± SD of triplicates.

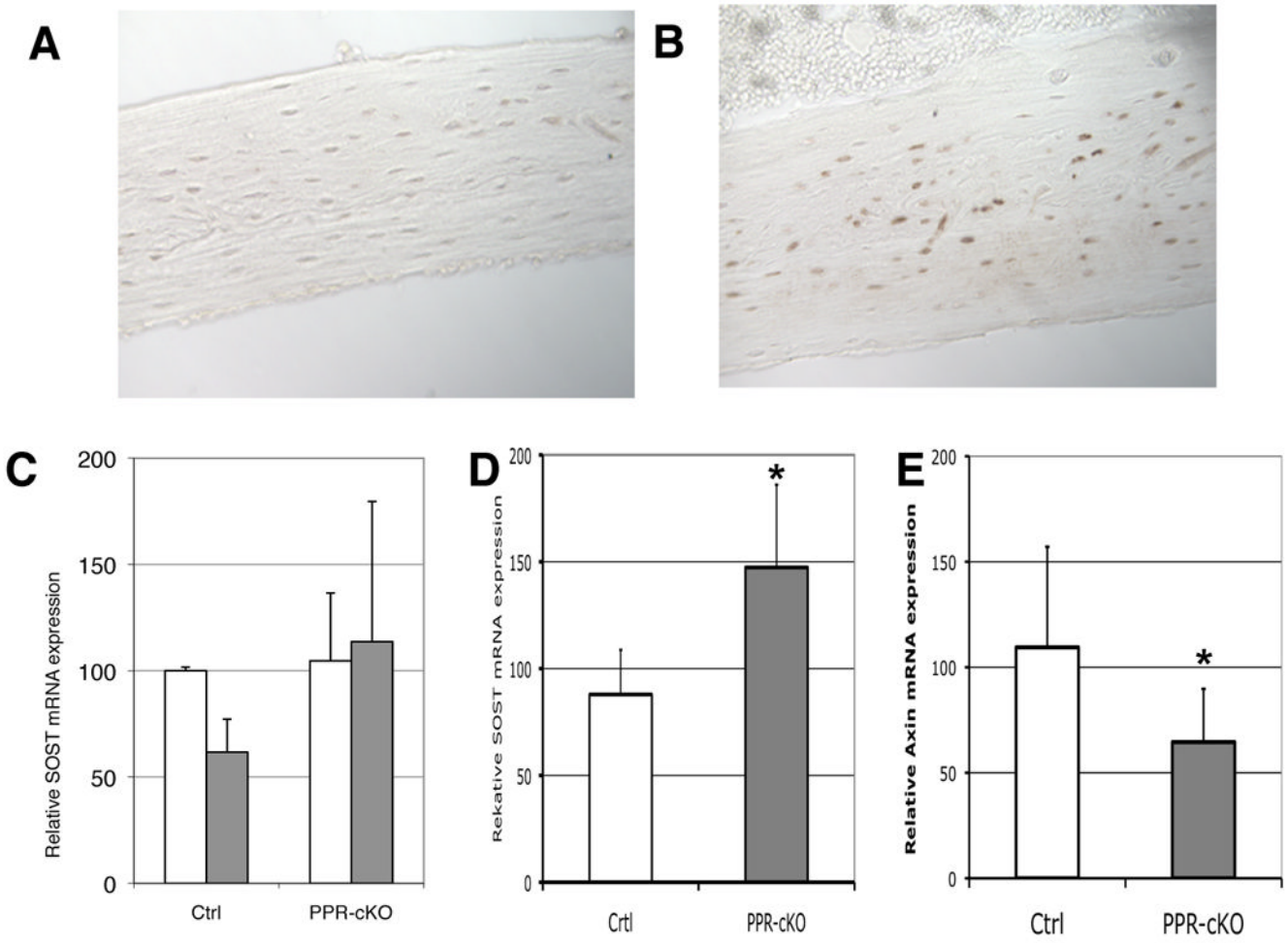

Figure 4. Sost and Sclerostin expression in Ocy-PPR^{cKO}

Immunohistochemisty for sclerostin was performed on sections of bone isolated from Ocy-PPR^{cKO} (A) and littermate controls (B) pretreated with 0.5 mg tamoxifen 3 × week for 4 weeks prior to acute sc injection with 300μg/kg of PTH(1-34). Mice were sacrificed 1 hr after the hormone injection. C) Real-time qPCR of SOST mRNA from femurs of control littermates (Ctrl) and Ocy-PPR^{cKO} (PPR-cKO) acutely injected with 300μg/kg of PTH(1-34)(grey bars) or vehicle alone (open bars). Data are expressed as percentage of vehicle-treated mice and normalized for GAPDH. D) Real-time qPCR of SOST mRNA from femurs of 4-6 weeks Ocy-PPR^{cKO} (PPR-cKO n=9) and control littermates (Ctrl n=8). * $p<0.005$. E) Real-time qPCR of Axin-2 mRNA from femurs of 4-6 weeks Ocy-PPR^{cKO} (PPR-cKO n=7) and control littermates (WT n=7). * $p<0.05$.

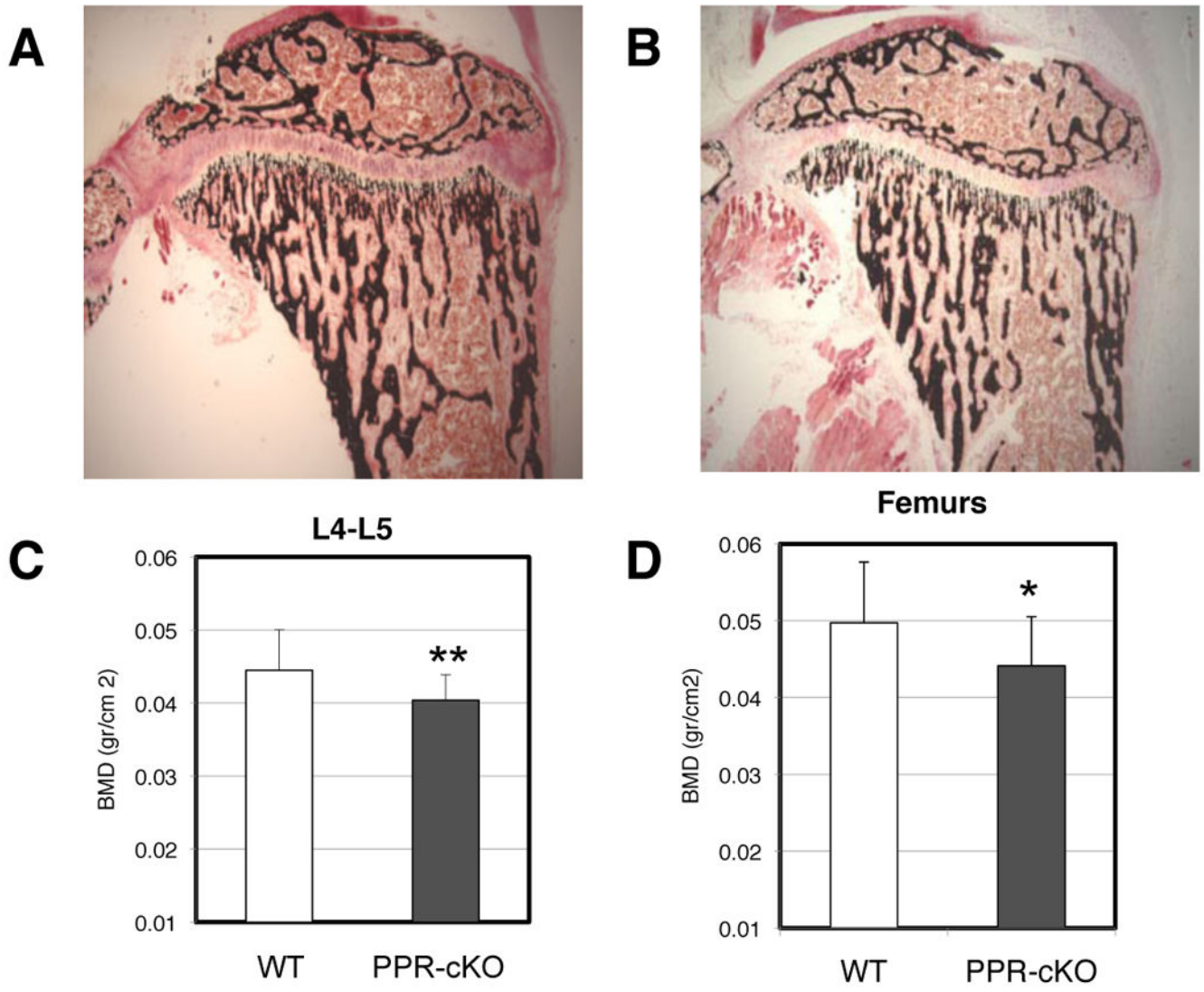

Figure 5. Osteopenia in Ocy-PPR^{cKO}

Von Kossa (A and B) staining of 3-4 weeks old tibia of controls (A) and Ocy-PPR^{cKO} (B) mice. Mice were injected with tamoxifen as described in Figure 2. Ocy-PPR^{cKO} animals demonstrated a decrease in trabecular bone and a delay in secondary ossification center. C and D) Low Bone Mineral density in Ocy-PPR^{cKO}. BMD of vertebral bodies (L4-L5)(E) and femurs (F) of Ocy-PPR^{cKO} (n=11) and controls (n=13) females. BMD was measured by DXA on isolated bones. Data are expressed as mean ± SD. * $p<0.1$ ** $p< 0.05$.

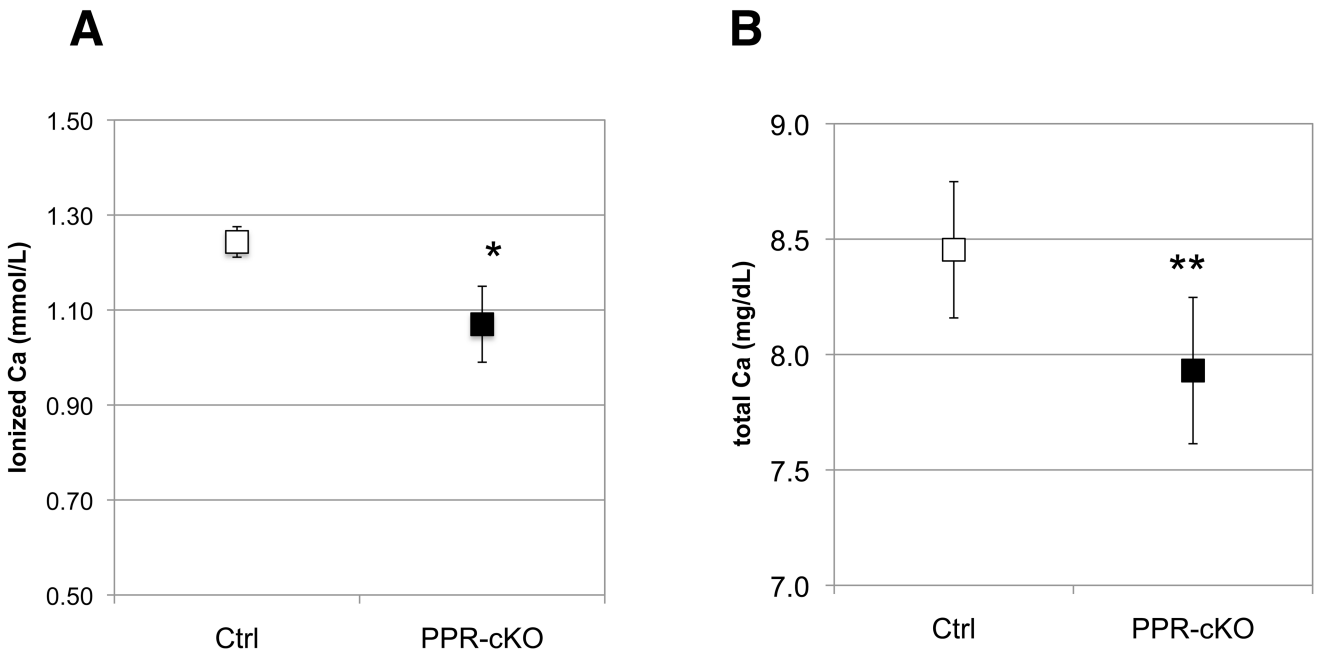

Figure 6. Plasma ionized and total calcium levels in Ocy-PPR^{cKO}(PPR-KO) and littermate controls (Ctrl) mice

Six weeks old mice were treated with 0.5 mg tamoxifen 3 times/week for 3 weeks and challenged with a low calcium diet for 2 weeks. Data are expressed as mean ± SD. Blood was collected at the end of the 3 weeks and analyzed for calcium content. Data are expressed as mean ± SD Ocy-PPR^{cKO} n=5, controls n=3 * $p<0.05$. A) ionized calcium; B) total calcium.